JOURNAL OF SPACECRAFT AND ROCKETS
Vol. 36, No. 6, November–December 1999

Surface Heating Effects of X-33 Vehicle Thermal-Protection-System Panel Bowing

Grant Palmer*
NASA Ames Research Center, Moffett Field, California 94035
Dean Kontinos*
Thermosciences Institute, Moffett Field, California 94035
and
Brian Sherman†
BF Goodrich Company, Chula Vista, California 91910

The thermal protection system on the windward side of the Lockheed Martin X-33 technology demonstrator vehicle consists largely of metallic panels. As the vehicle travels through the Earth's atmosphere at hypersonic speeds, thermal gradients between the top and bottom face sheets of the honeycomb panels cause them to bow. This study uses Navier–Stokes flow analysis to assess the effects of panel bowing on the surface heating of the vehicle. Analysis is performed at key locations on the design trajectory. A series of surface heating augmentation factors are presented that provide the increase or decrease in heating rate as a function of bow height. The existence of reverse flow at the panel interfaces because of panel bowing is demonstrated.

Nomenclature

D = diffusion coefficient, m^2/s
h = specific enthalpy, J/kg
M = molar mass, kg/mole
Ma = Mach number
q = heat flux, W/cm^2
R = Universal Gas Constant, 8.3144 J/mole-K
Re_θ = boundary-layer-edge Reynolds number
T = temperature, K
u = velocity, m/s
Z = bifurcation mass fraction
γ_s = recombination coefficient
ε = emissivity
η = direction normal to vehicle surface
κ = thermal conductivity of gas, W/m-K
ρ = density, kg/m^3
σ = Stefan–Boltzmann constant, $5.667e-8$ W/m^2-K^4

Subscripts

s = species
w = wall

Introduction

THE X-33 vehicle is a half-scale single-stage-to-orbit (SSTO) reusable launch vehicle (RLV) technology demonstrator being built under a cooperative agreement between Lockheed Martin and NASA. The vehicle is 20.4 m long and 20.7 m wide and has a gross takeoff weight of 600,600 kg. It is powered by two liquid-hydrogen/liquid-oxygen linear aerospike engines. Scheduled for first launch in 2000, the X-33 will demonstrate the enabling technology to construct a full-scale SSTO RLV[1] in the early part of the 21st century.

The thermal protection system (TPS) on the Space Shuttle orbiter is ceramic-based and requires significant maintenance between flights. The X-33 vehicle will use a metallic TPS, the first time a metallic system will be used on a flight vehicle. The metallic system was chosen because of its durability, moisture resistance, and lower life-cycle costs with respect to existing ceramic tile designs. The metallic TPS is designed to be reusable, low weight, low maintenance, and of sufficient strength to accommodate the aerodynamic and thermal loads encountered during ascent and reentry. There are two types of metallic systems being employed on the X-33, one made from PM-1000[2,3] and the other from INCO 617.[4] Both are of similar construction, with the PM-1000 material reserved for the higher temperature areas of the vehicle.

The TPS layout on the windward surface of the X-33 is shown in Fig. 1. Each TPS panel consists of outer and inner metallic face sheets surrounding a metallic honeycomb core. Beneath the inner face sheet is a layer of insulation contained within an Inconel foil bag that is attached to the back of the honeycomb panels. The insulation is sized to maintain the vehicle substructure and tank insulation below 450 K. The TPS panels are attached to the vehicle substructure via a standoff at each corner of the panel. The honeycomb construction and geometry is typical of that found on existing commercial and military aircraft; however, the material gauges are somewhat smaller to minimize weight.

The honeycomb materials were selected based on their strength and creep properties at high temperatures. However, one problem inherent to honeycomb panels is bowing caused by thermal gradients. The equivalent thermal conductivity of honeycomb panels is generally poor, consequently, when heated from one side, there can exist large thermal gradients through the panel. The aeroheating rates occurring on the X-33 during ascent and descent are high enough to produce gradients on the order of 170–220 K through the panel. Increasing the honeycomb facesheet temperature produces an in-plane expansion of the facesheet material. When the temperature of the inside facesheet lags that of the outer, there will also be a similar lag in the facesheet expansion. This nonuniform expansion of the honeycomb facesheets causes the panel to bow. When the temperature of the outer facesheet is greater than that of the inner facesheet, the panel bows in the outward direction. When the temperature of the inner facesheet is higher than that of the outer facesheet, the panel bows inward.

Panel bowing, into and out of the local flowfield, results in a change to the local heating rates. Depending on the location on the panel and whether the panel is bowing inward or outward, the

Presented as Paper 98-0865 at the AIAA 36th Aerospace Sciences Meeting, Reno, NV, 12–15 January 1998; received 15 May 1998; revision received 27 May 1999; accepted for publication 1 June 1999.

*Senior Research Scientist. Senior Member AIAA.
†Staff Engineer.

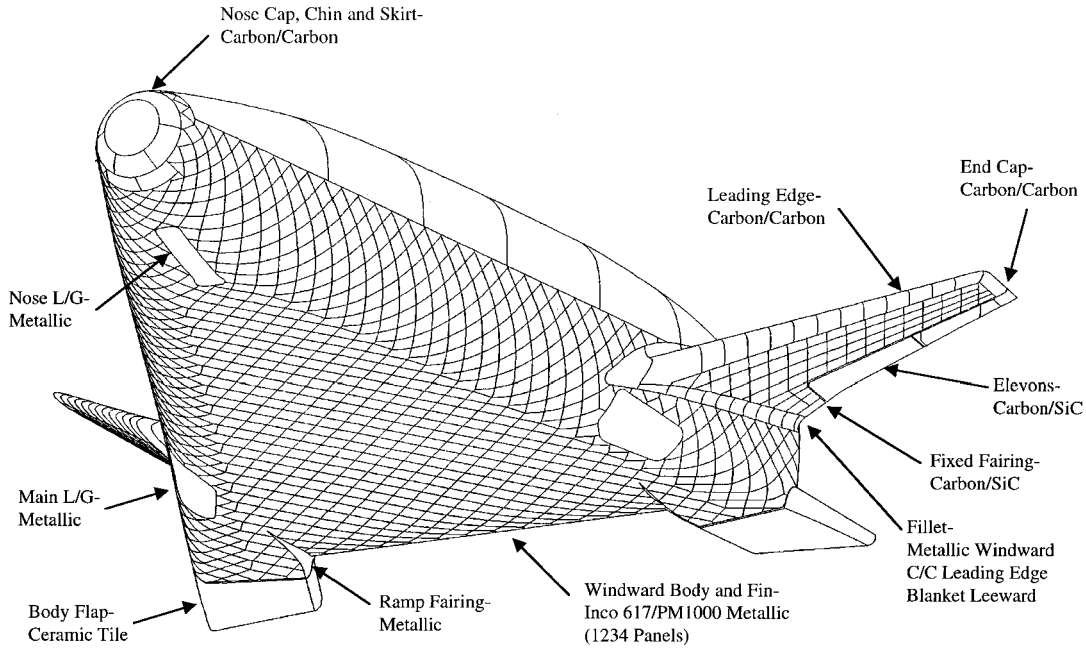

Fig. 1 X-33 windward surface TPS configuration.

heating rate and surface temperature can increase or decrease from the nominal value. This study uses Navier–Stokes computational fluid dynamic (CFD) analysis to determine heating amplification factors for various levels of panel bowing. These factors are applied to the undeflected heat rates to determine the panel temperatures during flight. The heating augmentation factors, along with the acreage aerothermal CFD analysis from Ref. 5, are used to generate the aerothermal database that was used to design the TPS of the X-33 vehicle.[6] The panel bowing data are also used by Kontinos and Palmer[7] in a more rigorous investigation of the metallic TPS panel bowing phenomenon that includes the entire panel-lattice-substructure stackup.

Methodology

The flow solutions are computed using GASP version 3 (Ref. 8). GASP is an established commercial Navier–Stokes flow solver that has been applied to a wide array of internal and external flow problems.[9–12] Solutions using GASP have been validated against Space Shuttle flight data[9,10] and have also been applied to generate the aerothermodynamic CFD solutions used in the design of the X-33 vehicle.[5] GASP solves the full Navier–Stokes equations that model the conservation of density, momentum, and energy using a variety of differencing schemes. It has a number of built-in chemistry and turbulence models and uses dynamic memory allocation to reduce run-time memory requirements.

Third-order spatially accurate van Leer flux-vector splitting[8] is used to difference the inviscid fluxes. Viscous terms are evaluated in all three coordinate directions. A five species, finite-rate, reacting gas, air chemistry model is used for all computations. The reaction-rate model is that of Park.[13] The species specific heats and enthalpies are obtained by assuming the internal energy modes are in translational, rotational, and vibrational equilibrium. Species viscosity is obtained using Blottner curve fits.[14] Species thermal conductivity is calculated using Eucken's relation.[15] Mixture viscosity and thermal conductivity are obtained using Wilke's mixing rule.[16] Species diffusion is assumed to be binary. The diffusion coefficients are obtained by assuming a constant Schmidt number. The turbulent flow solutions use the Baldwin–Lomax turbulence model[17] with a correction for compressibility effects.

The surface temperature is computed by solving an energy balance at the vehicle surface[11]:

$$\kappa\frac{\partial T}{\partial \eta}+\sum_{s=1}^{\text{nspc}}\rho D h_s\frac{\partial Z_s}{\partial \eta}=\sigma\varepsilon T_w^4 \tag{1}$$

For the calculations presented in this study, a constant emissivity of 0.85 is applied to the entire configuration. A more rigorous analysis of the panel-bowing phenomenon that includes in-depth conduction into the TPS stack-up is presented in Ref. 7.

The species diffusive flux is modeled using first-order reaction rates[11]:

$$\rho_s u_s=-\rho D_s\frac{\partial c_s}{\partial r}=\rho_s\gamma_s\sqrt{\frac{RT_w}{2\pi M_s}} \tag{2}$$

The wall is assumed to be fully catalytic, and so $\gamma_s=1$.

The computations were performed axisymmetrically using the windward centerline as the defining curve. The surface and volume grids used by the Navier–Stokes flow solver are generated from IGES geometry data using the GRIDGEN[18] grid generator. The X-33 analysis presented in this paper focuses on the forebody region of the vehicle. A hyperbolic tangent function is used to distribute grid points normal to the body surface. The first grid spacing off the body surface is set to $1.0e{-}6$ m. The flow problems investigated in this study are axisymmetric, but the flow solver is three dimensional so three-dimensional grids are generated with two symmetric circumferential planes. The OUTBOUND feature of the SAGE[19] adaptive grid code is used to conform the outer boundary of the grids to the shape of the bow shock wave.

There are certain limitations and assumptions inherent in this work. The bowed-panel geometries used in the parametric CFD analysis are generic in nature. The actual shape of the bowed panels on the X-33 vehicle will be different than the simplified configurations used in this study. Another uncertainty resides in the axisymmetric assumption. This assumption is made because of resource and schedule limitations, but the actual flow will have a three-dimensional crossflow component. Generally speaking, a two-dimensional object, such as a cylinder, will experience slightly less heating than its three-dimensional counterpart, a sphere. However, results from Ref. 7 indicate that the computed streamwise heating-rate profile along the center of a three-dimensional panel is the same shape as that produced by the axisymmetric solution, and the maximum and minimum values are of similar magnitude for a given bow height.

Results

Computations for the X-33 panel bowing analysis are performed at the trajectory points shown in Table 1. The 353-s point is the expected peak laminar heating-rate point. The 392-s point, when the vehicle is traveling at Mach 10, is a conservative estimate of the

Table 1 Freestream conditions

Time, s	Altitude, km	Density, kg/m^3	Mach	Angle of attack
353	53.4	6.81e−4	11.4	35.8
392	49.6	1.08e−3	10.0	20.0
465	45.0	1.90e−3	8.5	16.4

earliest trajectory point where the vehicle may experience turbulent flow over most of its surface. This assumption is based on freestream Reynolds number and experimental Re_θ/Ma correlations. The 465-s point is the expected point of peak negative panel bowing.

Panel Bowing: Comparison with Experiment

Tests were conducted in the NASA Langley Research Center 8-Foot High Temperature Tunnel at a Mach number of 6.5 to determine the surface heating effects of spherical protruberances mounted on a flat-plate test apparatus.[20] The purpose of the experiment was to simulate the effects of a thermally bowed metallic TPS tile. The experimental configuration is very similar to that used in this study, and so an attempt was made to reproduce the experimental results.

Computations are performed for dome heights of 0.005 and 0.01 m. The diameter of the dome is 0.3556 m. The domes are instrumented with pressure transducers and thermocouples to provide pressure and heat flux data. Boundary-layer probe measurements confirm that the undisturbed flow over the test apparatus is laminar. Turbulent data are also obtained using flow trips located 0.13 m aft of the 0.01-m-radius blunt leading edge.

The test gas consisted of the combustion products of methane and air. The total temperatures for the three runs (flat plate, 0.005-m dome, 0.01-m dome) range from 1856 to 1983 K. Total pressures range from 2.62e+6 to 2.98e+6 Pa. Freestream Mach numbers range from 6.54 to 6.59. All tests are performed at an angle of attack of 5 deg.

The ratio of the surface heating rate on the dome over the surface heating rate on the flat plate are shown in Fig. 2. The computed heating ratio for the 0.01-m dome is very close to the experimental data. The peak heating ratio is slightly underpredicted, and the computed location of the peak is slightly upstream of the experimental results. The maximum discrepancy between the computational and experimental heating ratios for both cases is less than 10%.

The maximum computational heating rate ratios are 1.25 for the 0.005-m dome and 1.8 for the 0.01-m dome. The ratio of dome height to dome diameter for these two cases is 0.014 and 0.028, respectively. Olsen and Smith[21] performed an analytical analysis on the same flat-plate-with-dome protuberance. They used freestream conditions corresponding to Mach 7 flow at 36.6-km altitude. For a dome height to dome diameter ratio of 0.021, they computed a maximum heating ratio of 1.4, which is consistent with the values computed in this study.

Panel Bowing: Parametric Analysis

Three 0.4572-m panels are modeled along the windward centerline of the X-33 vehicle. The leading edge of the first panel is 0.2286 m aft of the carbon-carbon nosecap. The panels are assumed to be attached to the underlying support structure 0.0381 m from the edge of the panel. Figure 3 shows a schematic of one of the TPS panels under a positive deflection. The assumption is made that $\frac{5}{6}$ of the overall panel deflection will occur outward at the panel midpoint. The remaining $\frac{1}{6}$ of the overall panel deflection occurs inward at the panel edge. The shape of the deflected panels is assumed to be spherical with the maximum deflection in the center of the panel. This bowed shape corresponds to a flat TPS panel under a uniform surface temperature distribution. The spherical-shape assumption is a simplification in that the panels may have some break in curvature and will certainly experience a nonuniform temperature distribution, but even under these conditions the bowing shape is approximately spherical in nature.

A parametric study of surface heating rate as a function of panel-deflection magnitude is performed. Computations are performed for the nominal (unbowed) surface and for six different levels of panel-deflection magnitude at two trajectory points. To make

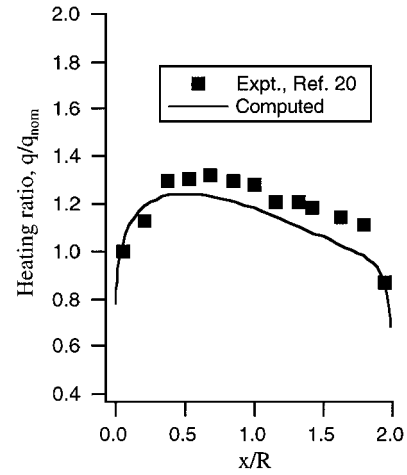

a) δ = 0.005 m (δ/D = 0.014)

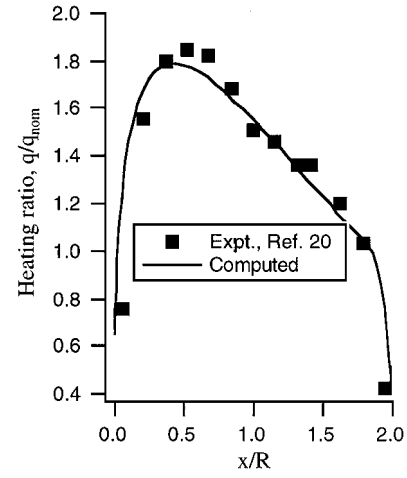

b) δ = 0.01 m (δ/D = 0.028)

Fig. 2 Comparison with experiment: spherical dome protuberances on a flat plate.

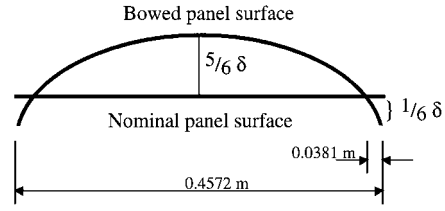

Fig. 3 Schematic of bowed-panel configuration.

the study computationally feasible, an axisymmetric analysis is performed using the windward centerline of the vehicle as the defining curve. To simulate the proper angle of attack at the peak heating and Mach 10 turbulent trajectory points, the axisymmetric grids are rotated by an amount equal to the angle of attack.

A grid sensitivity study is undertaken to determine a surface grid that would minimize grid dependence of the solution while maintaining a reasonable number of surface grid points. The results for a 0.0152-m panel deflection at the peak heating point are shown in Fig. 4. Using 9 or 17 equispaced points to represent the surface of each panel did not eliminate the grid dependence of the solution. Using 33 points to represent the surface of each panel with the panel-edge grid spacing, one-half the average grid spacing gave a solution very similar to that using 65 points per panel at half the computational cost. This distribution is used for all subsequent computations.

Figure 5 shows solutions at the peak heating point of the nominal Malmstrom 4 trajectory. Solutions are computed for the nominal surface and for panel deflections ranging from 0.003 to 0.0152 m.

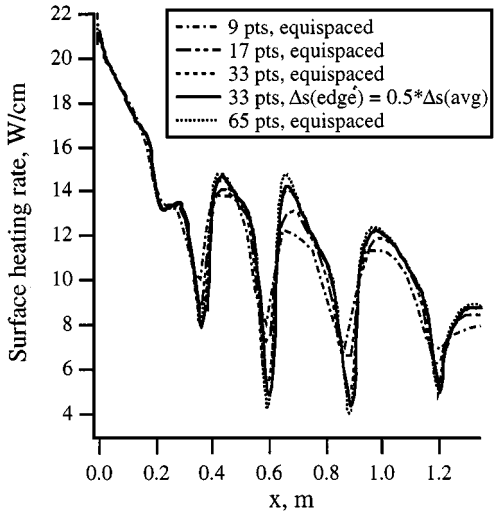

Fig. 4 Grid sensitivity study.

The maximum panel deflection is expected to be less than 0.0152 m. Figure 5a shows the absolute value of surface heating rate, whereas Fig. 5b shows the ratio of the deflected surface to nominal surface heating rate. The figures show a reduction in surface heating near, but not at, the panel edges and an increase in heating near the panel center caused by panel deflection. There is separation once the flow crosses the apex of the bowed panel and reattachment on the upward face of the next bowed panel. The maximum positive and negative heating spikes coincide with the separation and reattachment points. The 0.0152-m panel-deflection case shows a maximum heating augmentation factor of 1.26.

An examination of Fig. 5b indicates that, generally speaking, the maximum heating ratio value increases with each downstream panel. An early study that modeled nine panels showed that the peak heating ratio value did not continue to increase but fell into a pattern of rising and falling heating ratio peak values. The nonuniform peak values suggest there is an effect on the heating rate perturbation on a given panel because of the upstream panels. Applying the maximum heating-rate augmentation factor for all panels would be a conservative approach.

The same set of computations is performed at the Mach 10 turbulent point. The results are shown in Fig. 6. The panel edges are at different locations because this distance is measured from the stagnation point, which is a function of angle of attack. The maximum heating augmentation factor for the 0.0152-m panel deflection is 1.08. Figure 7 compares the surface heating-rate profiles for the 0.0152-m panel deflection at the peak heating and Mach 10 turbulent trajectory points. In this figure the panel edges of the Mach 10 turbulent data are shifted to line up with the peak heating panel edges. The disturbance in the heating-rate profile caused by panel bowing is less at the Mach 10 turbulent point than at the peak heating point. The higher laminar heating augmentation is also seen in the experimental data of Ref. 20, where the heating-rate ratios for a given dome height are higher when the flow is laminar than it is for turbulent flow. A summary of the maximum heating augmentation factors for the peak heating and Mach 10 turbulent cases are contained in Table 2.

One of the consequences of panel bowing is that the flow coming over the apex of the bowed panel separates and a region of reverse flow develops at the panel edge. This reverse flow may have consequences with regard to the panel-edge seal design. This phenomenon, although seen with the high-resolution axisymmetric computations, was not found in lower resolution three-dimensional solutions, so that it is not clear if and to what extent flow recirculation occurs.

During the descent, heat soak into the TPS panel can cause the inner facesheet to be at a higher temperature than the outer facesheet. When this happens, the TPS panels will bow inward, causing peaks at the panel edges. Computations were performed at the point where the maximum negative bowing is expected to occur. The magnitude

Table 2 Maximum heating augmentation factors, outward panel bowing

Cases	Deflection magnitude, m				
	3.05*e*−3	6.10*e*−3	9.14*e*−3	1.22*e*−2	1.52*e*−2
Peak heating	1.05	1.09	1.13	1.18	1.26
Mach 10 turbulent	1.02	1.05	1.07	1.09	1.12

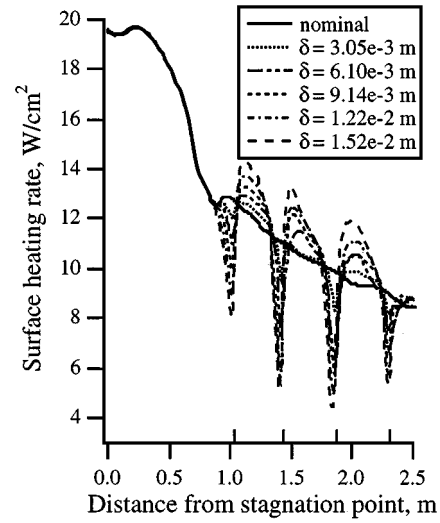

a) Surface heating rate

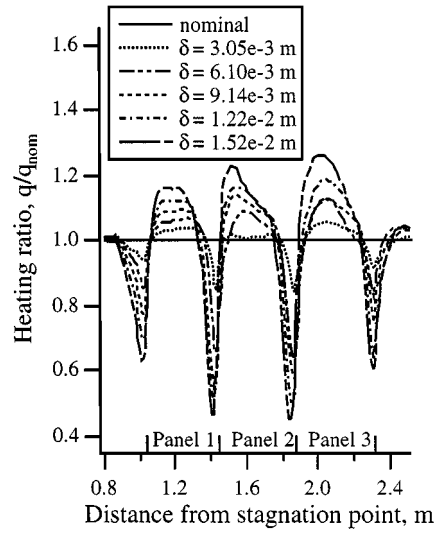

b) Heating ratio q/q_{nom}

Fig. 5 Effect of panel bowing: 353-s trajectory point.

of negative bowing modeled ranged from 0.00229 to 0.0137 m. The results are shown in Fig. 8. Sharp peaks in surface heating rate occur at the panel edges because of negative panel bowing, whereas the panel centers are cooler than the nominal surface solution. The maximum heating augmentation factors as a function of deflection magnitude are listed here:

1) For a negative deflection magnitude of 2.29*e*−3 m, the heating augmentation factor is 1.04.

2) For a negative deflection magnitude of 4.57*e*−3, the heating augmentation factor is 1.11.

3) For a negative deflection magnitude of 6.86*e*−3, the heating augmentation factor is 1.18.

4) For a negative deflection magnitude of 9.14*e*−3, the heating augmentation factor is 1.24.

5) For a negative deflection magnitude of 1.37*e*−2, the heating augmentation factor is 1.38.

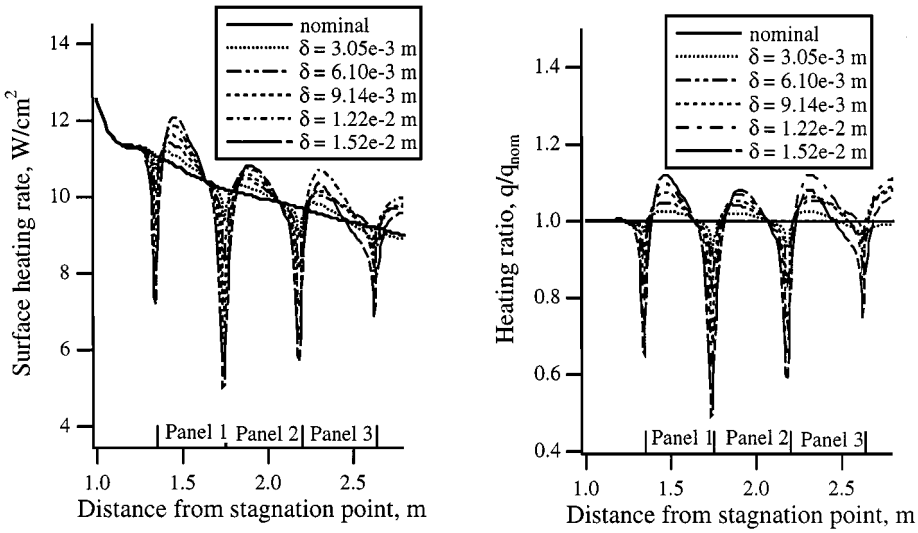

a) Surface heating rate b) Heating ratio q/q_{nom}

Fig. 6 Effect of panel bowing: Mach 10 turbulent trajectory point.

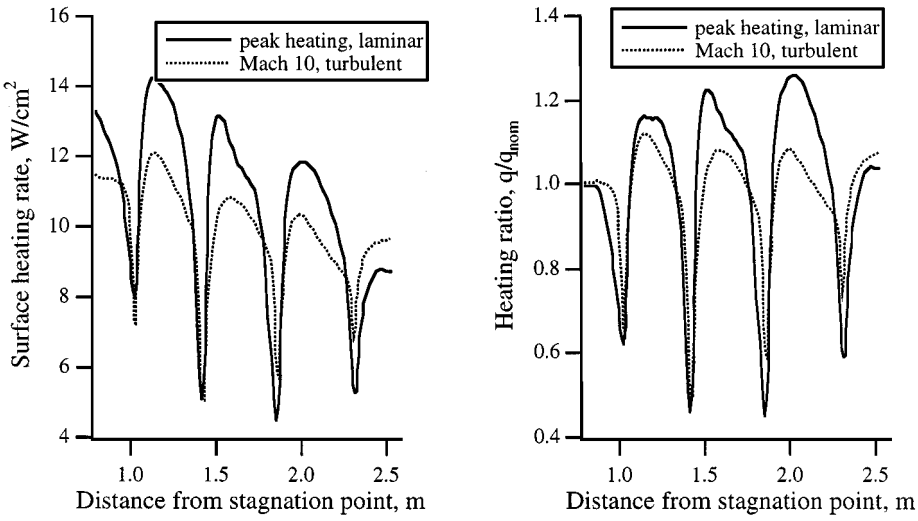

a) Surface heating rate b) Heating ratio q/q_{nom}

Fig. 7 Comparisons of peak heating and Mach 10 turbulent results.

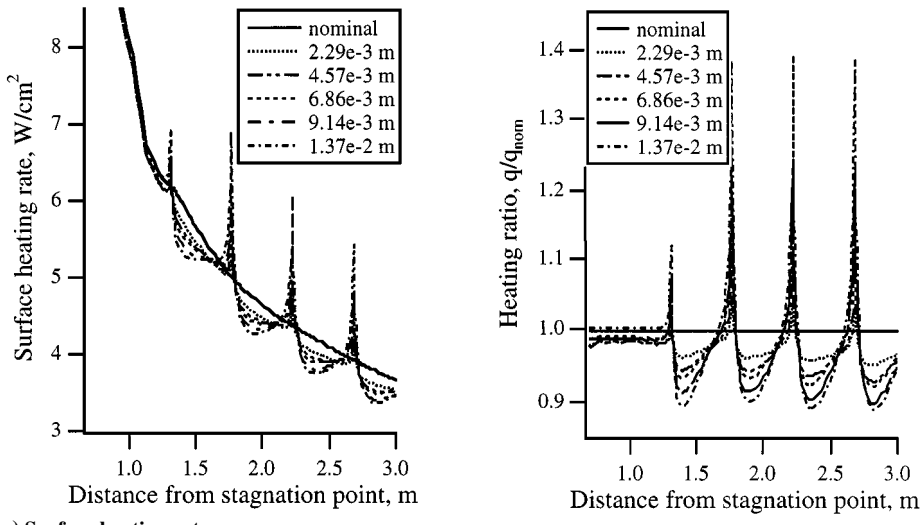

a) Surface heating rate b) Heating ratio q/q_{nom}

Fig. 8 Effect of panel bowing: maximum negative bowing trajectory point.

For a given level of panel bowing, the heating augmentation factors are greater for inward bowing than they are for outward bowing. However, the inward bowing occurs at a point in the trajectory of relatively low nominal heating. The augmented negative bowing heating rates are below the peak heating nominal values.

Conclusion

A simplified model is developed and detailed, and parametric computations are performed to assess the effects of TPS panel bowing on the surface heating rate of the X-33 vehicle. Navier–Stokes flow analysis is performed at three locations of the X-33 nominal Malmstrom 4 trajectory. A series of surface heating augmentation factors are presented that provide the increase in surface heating as a function of bow height. The existence of reverse flow at the panel interfaces caused by panel bowing is demonstrated in the axisymmetric computations but is not seen in lower-resolution three-dimensional computations. The heating augmentation factors presented are for generic surface protuberances and should be viewed with the limitations of the solution methodology in mind.

Acknowledgments

This work was supported under NASA Cooperative Agreement NCC8-115 and NASA Ames Research Center Task Agreement ARC-04. Support was also provided under NASA Contract NAS2-14031 to Eloret Institute. Computer time was provided by the NASA Numerical Aerodynamic Simulation Supercomputer Facility at NASA Ames Research Center.

References

[1]Urie, D. M., and Elving, J. D., "Innovative Economic Development and Technology Integration for Single Stage to Orbit (SSTO) Concepts," AIAA Paper 95-0279, Jan. 1995.

[2]Norris, B., "Fabrication and Evaluation of ODS Structural Sandwich Panels for Lightweight, Very High Temperature, Aerospace Applications," *Proceedings of the 14th International Plansee Seminar*, RM 28, 1997, p. 263.

[3]Jager, H., et al., "Forging of Nickelbase-ODS-Alloys," *Proceedings of the 13th International Plansee Seminar*, RM 90, 1993, p. 782.

[4]Inco Alloys Handbook, "Inconel Alloy 617," Inco Alloys International, Inc., Publication IAI-38, Huntington, WV, 1988, pp. 55–60.

[5]Prabhu, D. K., Loomis, M. P., Venkatapathy, E., Polsky, S., Papadopoulos, P., Davies, C., and Henline, B., "X-33 Aerothermal Environment Simulations and Aerothermodynamic Design," AIAA Paper 98-0868, Jan. 1998.

[6]Bowles, J., and Henline, W., "Development of an Aerothermodynamic Environments Database for the Integrated Design of the Prototype Flight Tests Vehicle," AIAA Paper 98-0870, Jan. 1998.

[7]Kontinos, D., and Palmer, G., "Numerical Simulation of Metallic TPS Panel Bowing," AIAA Paper 98-0866, Jan. 1998.

[8]Walters, R. W., Slack, D. C., Cinnella, P., Aplebaum, M., and Frost, C., "A User's Guide to GASP," Dept. of Aeronautical and Ocean Engineering, Virginia Polytechnic Inst. and State Univ., Research Rept. on NASA Grants NAG-1-766 and NAG-1-1045, Blacksburg, VA, Nov. 1990.

[9]Gnoffo, P., Weilmuenster, K., and Alter, S., "Multiblock Analysis for Shuttle Orbiter Re-Entry Heating from Mach 24 to Mach 12," *Journal of Spacecraft and Rockets*, Vol. 31, No. 3, 1994, pp. 367–377.

[10]Olynick, D., and Tam, T., "Trajectory-Based Validation of the Shuttle Heating Environment," *Journal of Spacecraft and Rockets*, Vol. 34, No. 2, 1997, pp. 172–181.

[11]Olynick, D. R., and Henline, W. D., "Navier–Stokes Heating Calculations for Benchmark Thermal Protection System Sizing," *Journal of Spacecraft and Rockets*, Vol. 33, No. 6, 1996, pp. 807–814.

[12]Palmer, G. E., Henline, W. D., Olynick, D. R., and Milos, F. S., "High-Fidelity Thermal Protection System Sizing of Reusable Launch Vehicle," *Journal of Spacecraft and Rockets*, Vol. 34, No. 5, 1997, pp. 577–583.

[13]Park, C., "On Convergence of Computation of Chemically Reacting Flows," AIAA Paper 85-0247, Jan. 1985.

[14]Blottner, F. G., Johnson, M., and Ellis, M., "Chemically Reacting Viscous Flow Program for Multi-Component Gas Mixtures," Sandia Lab., SC-RR-70-754, Albuquerque, NM, Sept. 1971.

[15]Vincenti, W. G., and Kruger, C. H., *Introduction to Physical Gas Dynamics*, 1st ed., Krieger, Malabar, FL, 1965, p. 21.

[16]Wilke, C. R., "A Viscous Equation for Gas Mixtures," *Journal of Computational Physics*, Vol. 18, No. 4, 1950, pp. 517–519.

[17]Baldwin, B., and Lomax, H., "Thin Layer Approximation and Algebraic Model for Separated Turbulent Flows," AIAA Paper 78-0257, Jan. 1978.

[18]Steinbrenner, J. P., and Chawner, J. R., "The GRIDGEN Version 9 Multiple Block Grid Generation Software," MDA Engineering, Inc., MDA Engineering Rept. 94-01, Arlington, TX, June 1994.

[19]Davies, C. B., and Venkatapathy, E., "The Multidimensional Self-Adaptive Grid Code, SAGEv2," NASA TM 110350, April 1995.

[20]Glass, C. E., and Hunt, L. R., "Aerothermal Tests of Spherical Dome Protuberances on a Flat Plate at a Mach Number of 6.5," NASA TP-2631, May 1986.

[21]Olsen, G. C., and Smith, R. E., "Analysis of Aerothermal Loads on Spherical Dome Protuberances," *AIAA Journal*, Vol. 23, No. 5, 1985, pp. 650–656.

B. A. Bhutta
Associate Editor